

Ionic Liquids Based Cocktails as a Composite Redox Electrolyte for Natural Dye-Sensitized Solar Cells

Ahmad Mudzakir^{a,*}, Asep Bayu Dani Nandiyanto^a, Heli Siti Halimatul Munawaroh^a,
Karina Mulya Rizky^a, Danar Wulan^a, Lafita Kaova Azyedara^a, Sendy Arfian Saputra^a

^a Departemen Pendidikan Kimia, Fakultas Pendidikan Matematika dan Ilmu Pengetahuan Alam, Universitas Pendidikan Indonesia, Bandung, 40154, Indonesia

Corresponding author: *mudzakir.kimia@upi.edu

Abstract — Fatty-imidazolium electrolytes, waste graphite dispersed composite electrolytes like cocktails (1,3-methyl octyl-1,2,3-benzotiazolium acetate–cis-oleyl-imidazolium iodide), and graphite exfoliation using cis-oleyl-imidazolium acetate have been studied to enhance the efficiency of a newly developing dye-sensitized solar cells (DSSCs). The DSSCs were fabricated in a sandwich structure and characterized using Solar Simulator. The graphite exfoliation was conducted by sonication and microwave energy, as well as the electrochemical method. Cis-oleyl-imidazolium iodide efficiency (0.53%) was highest than stearyl-imidazolium iodide and palmityl-imidazolium iodide because cis-oleyl-imidazolium iodide has a double bond and the longest alkyl chain which triggered a self-assembly structure formation and increased the rate of I^-/I^{3-} transport in cells. Then, the efficiency of DSSCs-based composite electrolytes was in the range of 0.020–0.203%. Dispersion of 0.05% of the graphite results in efficiency enhancement of about 100%, but the greater fraction (0.10%) of the graphite causes a poor performance (lower efficiency), possibly due to interference of the internal electron transportation routes in the DSSC by insoluble graphite. After exfoliation, the conductivity of synthetic graphite (11.58×10^{-1} S/cm), new battery graphite (9.32×10^{-1} S/cm), and battery waste graphite (7.96×10^{-1} S/cm) were increased respectively 10 times, 2 times, and 4 times from the graphite before exfoliation due to changes in crystallinity, the distance between layers, crystal size, formation of multilayer graphene, and the occurrence of π to π^* transition. This enhancement of solar conversion efficiency can give a new contribution to the development of DSSC.

Keywords— Dye-sensitized solar cell (DSSC); redox electrolyte; graphite; ionic liquids cocktails; composite electrolyte.

Manuscript received 13 Jan. 2022; revised 7 Feb. 2022; accepted 4 May 2022. Date of publication 31 Oct. 2022.
IJASEIT is licensed under a Creative Commons Attribution-Share Alike 4.0 International License.



I. INTRODUCTION

Sun is one of the energy sources that are very promising for the future because it has continuous electromagnetic radiation. Sun energy is used by a device named dye-sensitized solar cells (DSSCs) [1]-[3]. DSSC consists of a dye, an electrolyte, and a working and counter electrode [4]. It is a low-cost solar cell [5]. A dye can be adsorbed on a TiO_2 layer in a DSSC [6]. TiO_2 is coated on a conductive glass [7-9]. A redox couple is needed to operate a DSSC, and the most common redox couple for DSSCs is I^-/I_3^- [10]-[12]. The others are transition metals such as Co^{3+}/Co^{2+} [13]-[15] or Cu^{2+}/Cu^+ [16]-[18]. Those redox couples are also promising.

To obtain a high cell efficiency, an organic solvent must be incorporated into the formulation of the electrolyte [19]-[21]. According to recent studies [22], the ionic liquid compounds that are incorporated in DSSCs can be used to obtain high

efficiency. C_4 to C_{10} alkyl chains will form compounds with ionic liquids (ILs) characteristics, while compounds with longer alkyl chains than that will form liquid crystals [23]. The alkyl chain length of ILs indeed can affect the DSSC efficiency [24]. In addition, the double bond in the alkyl chain also significantly changes the space arrangement of the molecular system and reduces the packing efficiency. It leads to the low viscosity of ILs, which would increase the redox couple's diffusion [25]. The ionic liquid added to gel polymer electrolytes (GPEs) also increased the ionic conductivity because the mobile ions that hop to the vacant site were enhanced [26]. However, the backreaction in DSSC was known to cause decreasing energy conversion efficiency [27]-[29]. Thus, it needs to develop further.

It has been known that graphite is one of the promising materials for the counter electrode in DSSCs due to its notable electrical conductivity, although its electrocatalytic activity was low. Graphite composite-based counter electrode has

good resistance to corrosion, low cost, and easy fabrication. Therefore, it can enhance the photovoltaic performance [30]-[33]. Graphene-based materials also can enhance DSSC performance due to the improvement of hole transport for an optimum concentration in the I/I^3 [34]-[36]. This research aims to elaborate on a new composite as a redox electrolyte for DSSC. We used ionic liquid cocktails based on benzotriazolium acetate-cis-oleyl-imidazolium iodide and graphite as a composite electrolyte for DSSC. Besides that, fatty-imidazolium electrolytes and graphene exfoliation were also studied further. The novelty of this study was the use of sustainable ionic liquid based on fatty imidazolium and waste graphite as composite components.

II. MATERIALS AND METHODS

Fatty-imidazolium was synthesized based on the procedure that was modified from Bajpai and Tyagi [37] and 1,3-methyloctyl-1,2,3-benzotriazolium acetate ([MOBzt] CH_3COO) was synthesized based on the procedure that was modified from Forsyth and MacFarlane [38]. Fig. 1 shows the scheme of the experimental method in this research.

A. Materials

The materials used in this research were cis-oleic acid, stearic acid, palmitic acid, methyl iodide, diethylenetriamine, acetonitrile, methylene chloride, ethyl acetate, calcium oxide, methanol, n-hexane, 1H-benzotriazole, dimethyl sulfate, octyl bromide, NaOH, MgSO_4 , acetonitrile, ethanol, hydrochloric acid, silver nitrate, potassium thiocyanate, sodium acetate, silver acetate, $0.45\mu\text{m}$ cellulose-nitrate membrane, synthetic graphite, new batteries, waste battery, powder TiO_2 , polyvinyl alcohol, potassium iodide, iodine, scotch insulation, conductive glass (ITO), strawberry, and 0.005M Eosin Y.

B. Fabrication of DSSC Prototype Based on Fatty-Imidazolium Iodide Electrolytes

Fatty-imidazoline was synthesized by adding 40 mmol of fatty acids (cis-oleic acid, palmitic acid, and stearic acid) into 20 g of calcium oxide. The mixture was stirred and irradiated using a microwave at 800-850 W for 30 seconds to 3 minutes. After the mixture reached room temperature, 80 mL of ethyl acetate was added to the mixture. The mixture was refluxed at 40°C for 30 minutes. Then, the mixture was filtered in a hot state and the ethyl acetate was removed using an evaporator.

Fatty-imidazolium iodide was synthesized by adding 1-mole fatty-imidazoline, 2-mole methyl iodide, and methylene chloride as solvent into a flask that was covered with aluminum foil. The mixture was refluxed and stirred at 40°C for 4 hours. Then, the mixture was cooled to room temperature and dried by using an evaporator at a temperature of 80°C for 2-4 hours. The products must be stored in a dark and closed container.

The dye sensitizer for these fatty-imidazolium electrolytes was made from strawberry fruit extract. 20 g of strawberries were blended and added into 50 ml of methanol, 8 ml of acetic acid, and 42 ml of distilled water. The mixture was macerated for 24 hours and stored in a dark place. After that, the strawberry extract was filtered using gauze into a dark bottle.

The redox electrolytes consisted of a comparison electrolyte (0.2 M potassium iodide and 0.08 M iodide in 5

mL acetonitrile) and three other electrolytes (0.6 M of cis-oleyl-imidazolium iodide (Elt_1) or stearyl-imidazolium iodide (Elt_2) or palmityl-imidazolium iodide (Elt_3), 0.2 M potassium iodide, and 0.08 M iodide in 5mL acetonitrile).

The working electrode was started by dissolving 5 g polyvinyl alcohol in 50mL water. After that, 5 g TiO_2 was added to the suspension and stirred until the paste was formed. An area for TiO_2 deposition with a width of 1 cm above the conductive surface was formed on the TCO glass (with a dimension of about 2 x 2 cm). The side of the glass was affixed with tape as a barrier and a thickness of the paste was deposited. The paste was placed on the surface of the TCO glass and leveled. Then, the tape was removed. The paste on the glass was dried at $\pm 24^\circ\text{C}$ and sintered at 1500°C for 10 minutes. The glass was cooled to 800°C and immediately immersed in the dye for 2 hours and dried at $\pm 24^\circ\text{C}$.

The counter electrode was prepared by using wax soot to coat the conductive glass that was cut into a size of about 2 x 2 cm, then heated at a temperature of 450°C for 10 minutes. The DSSC prototype was fabricated by placing the counter electrode on the working electrode in a sandwich structure and clamping it with binder clips on both sides. Then, 2 drops of the electrolyte were dropped into the space between the electrodes.

C. Fabrication of DSSC Prototype Based on Graphite Waste Dispersed Composite Electrolytes

Cis-oleyl- imidazolium iodide was synthesized like the procedure above. Then, 1,3-methyloctyl-1,2,3-benzotriazolium acetate was synthesized by methylation of 1H-Benzotriazole first. 50 g of 1H-benzotriazole was dissolved in sodium hydroxide in water. 40 mL of dimethyl sulfate was added to the mixture and stirred for 24 hours at room temperature. After that, hydrochloric acid was added to the solution and extracted using ethyl acetate. The organic phase was added by anhydrous copper sulfate to remove water. Then, the mixture was filtered and evaporated at a temperature of $60\text{-}70^\circ\text{C}$. The evaporation product was put in the freezer to form 1-methyl-benzotriazole crystals. The crystals were filtered and then purified by recrystallization using n-hexane and decanted to remove impurities. After that, the solution was put into the freezer again until pure 1-methyl-benzotriazole crystals were obtained. After that, 1,3-methyloctyl-benzotriazolium bromide was synthesized by dissolving 10 g of 1-methyl benzotriazole crystals in acetonitrile. Then, 15 mL of octyl bromide was added and refluxed for 24 hours at $75\text{-}85^\circ\text{C}$. The reflux product was evaporated at a temperature of 80°C . Finally, 1,3-methyloctyl-benzotriazolium acetate was synthesized by adding 1.413 g of [MOBzt] Br into 0.840 g of CH_3COOAg in methanol and stirred for 6 hours at room temperature. The product was filtered and evaporated.

Graphite sample was obtained from waste batteries that were opened and therefore the graphite was taken. The dye sensitizer was 0.05 M Eosin Y. Composite redox electrolytes consisted of 0% of graphite (Elt_4) or 0.01% of graphite (Elt_5) or 0.05% of graphite (Elt_6) or 0.1% graphite (Elt_7), 10% of cis-oleyl imidazolium iodide and 90% of 1,3-methyloctyl-1,2,3-benzotriazolium acetate. For the DSSC fabrication was the same as the procedures above.

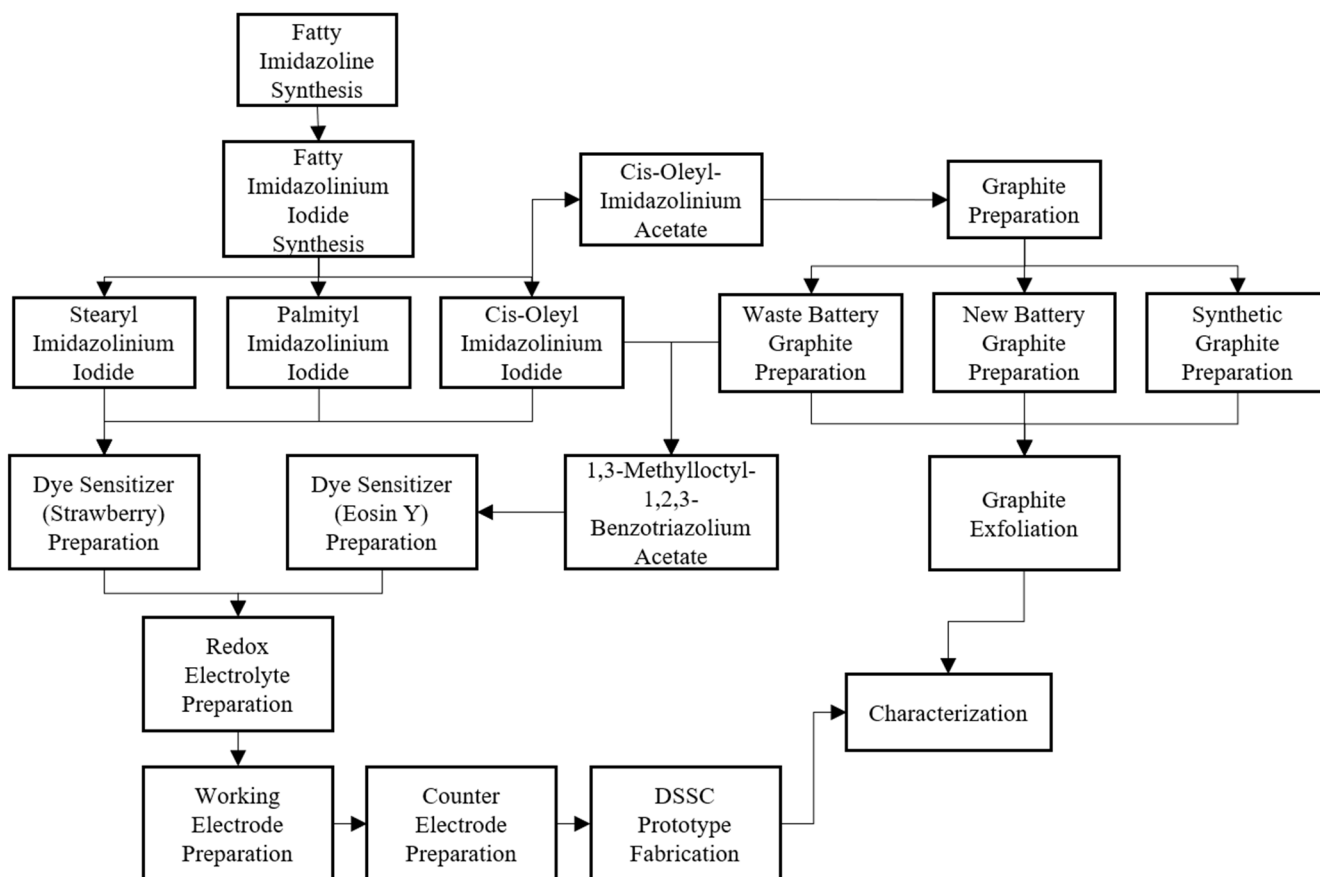


Fig. 1 Scheme of DSSCs prototype fabrication and graphite exfoliation

D. Exfoliation of Graphite into Graphene

Cis-oleyl-imidazolium acetate was synthesized by dissolving 10 mmol of cis-oleyl-imidazolium iodide in 100 mL of methanol and then 10 mmol of AgCH_3COO was added. The mixture was stirred for 4 hours. The product was decanted and filtered using a cellulose-nitrate (PTFE) membrane. The solvent in the filtrate was then evaporated by storing it in a fume hood until it was saturated. The graphite samples were obtained from synthetic graphite, new battery graphite, and waste battery graphite. Synthetic graphite has been in the form of a fine powder. New battery graphite and waste battery samples were taken from the battery electrodes and ground into a fine powder. Then, they dried in an oven at 400°C . The dried graphite samples were filtered using a 100-mesh sieve.

The first exfoliation used the dissolving method. 1 g of cis-oleyl-imidazolium-acetate were put into 5 vials. The three graphite samples were divided into 0.1%; 0.5%; 1%; 1.5%; and 2% of the total mass of the ionic liquid. The mixture was ultrasonically energized for 1-2 hours. Then, the products were put into a microwave at a low power of 100 W. During microwave heating, the vial containing the product was removed, shaken, and put back in the microwave until the graphite powder was completely dissolved.

The second exfoliation used the electrochemical method. This method used a graphite sample as the electrode while the cis-oleyl-imidazolium-acetate in water was the electrolyte. The graphite sample was made into a pellet before being used as an electrode. The electrode was clamped using a clamp that

has been connected to a cable and inserted into the electrolyte containing ionic liquid in water with a composition of 1:1. Static voltage (DC) of 15 V was applied. The mixture was separated by centrifugation at 15000 rpm and filtered to obtain the exfoliated graphite precipitate.

E. Characterization Methods

The structural characterization of the synthesized compounds was analyzed using Fourier Transform Infrared (FTIR) and Scanning Electron Microscopy (SEM). Melting temperature and clearing temperature were known through Differential Scanning Calorimetry (DSC). The absorption profile was analyzed using UV-Vis Spectrophotometer. Conductivity was measured using a digital multimeter or Electrochemical Impedance Spectroscopy (EIS). The crystallinity of graphite was analyzed using X-Ray Diffraction (XRD). Thermogravimetry and Differential Thermal Analysis (TG-DTA) were used to determine the decomposition temperature of graphite before and after the exfoliation. Current and voltage in the DSSC prototype were analyzed using Solar Simulator 100 mW/cm^2 or 16.6 mW/cm^2 . Detailed information on interpreting UV-Vis, FTIR, XRD, SEM, and TG-DTA is explained in our previous studies [39-43].

III. RESULTS AND DISCUSSION

A. Fabrication of DSSC Prototype Based on Fatty-Imidazolium Iodide Electrolytes

Fatty imidazoline was synthesized using the microwave irradiation method to speed up the reaction [37], while the

iodide anion function was to increase the rate of exchange reaction-diffusion I^-/I^{3-} [44]. Fig. 2 shows the comparison of the FTIR spectra of stearic acid, DETA, and stearyl-imidazolium iodide. The peak 3400 cm^{-1} indicated the presence of N-H group stretching. The peak at $< 3000\text{ cm}^{-1}$ indicated C-H sp^3 stretching and the peak at 1604 cm^{-1} indicated an amide group that overlaps with C=O. Based on the presence of those groups, the desired fatty imidazolium compounds have been successfully synthesized.

From Fig. 3, there were two endothermic peaks in the cis-oleyl-imidazolium iodide which indicated that it has a liquid crystal phase change range of 68.92°C ($82.58\text{--}151.50^\circ\text{C}$), while the two others did not show any change in the liquid crystal phase because they only have one peak (Fig. 4 and 5). This peak indicated a phase change from a solid to an ordinary isotropic liquid phase. The presence of double bonds in cis-oleyl alkyl causes the molecule to be bulkier than the stearyl and palmityl alkyls, which affect the width of the liquid crystal phase [25]. In addition, palmityl and stearyl have straight chains, which causes very strong intermolecular interactions so their physical appearances were also denser than cis-oleyl.

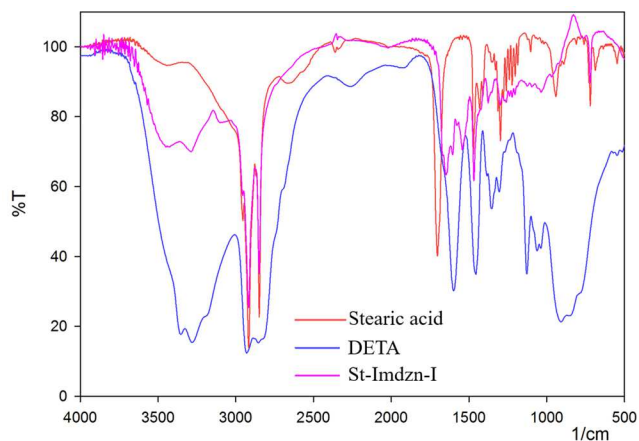


Fig. 2 Comparison of FTIR spectra of stearic acid, DETA, and stearyl-imidazolium iodide

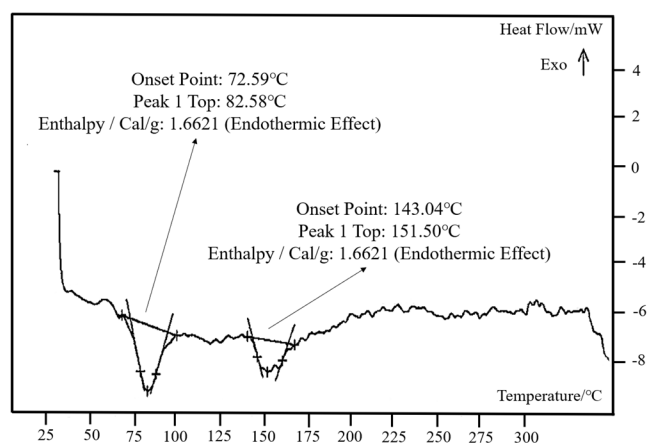


Fig. 3 DSC curve of cis-oleyl-imidazolium iodide

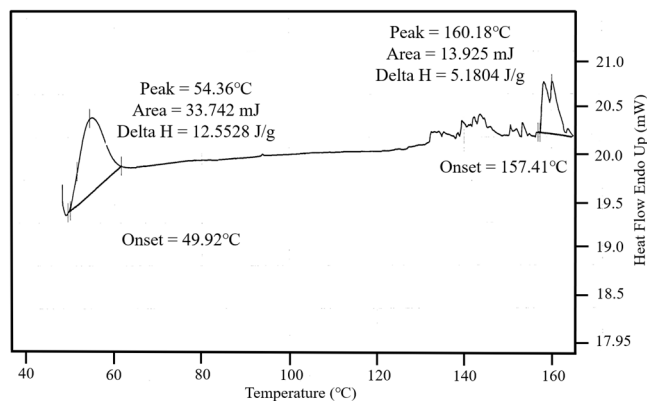


Fig. 4 DSC curve of palmityl-imidazolium iodide

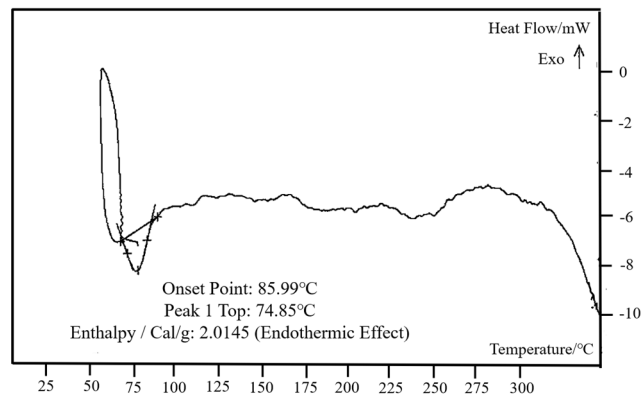


Fig. 5 DSC curve of stearyl-imidazolium iodide

Then, the UV-Vis absorption spectrum of the strawberry extract is shown in Fig. 6. The strawberry extract has a fairly wide absorption in the visible light region with maximum absorption at 499.5 nm . This means that the strawberry extract dye can be used as a photosensitizer in DSSC cells. However, when compared to the ruthenium complex dye [45], the absorption response of this strawberry extract dye is still relatively low, so the conversion current of the resulting solar cell will be lower. Meanwhile, Fig. 7 shows the FTIR spectrum of strawberry extract and indicated the presence of flavonoid derivative compounds. This compound plays an important role as a photosensitizer in DSSC cells.

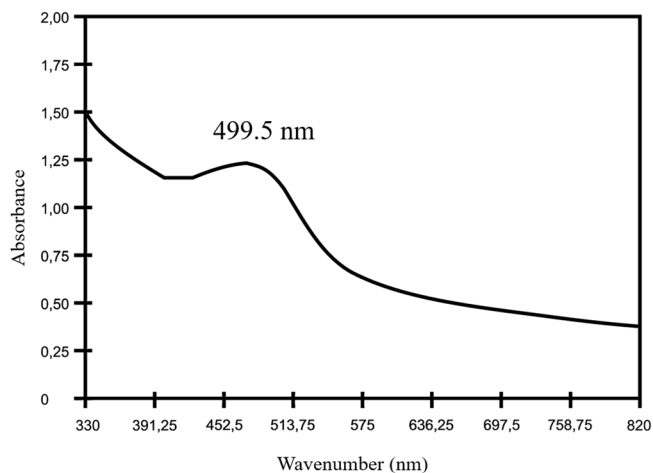


Fig. 6 UV-Vis's spectrum of strawberry extract

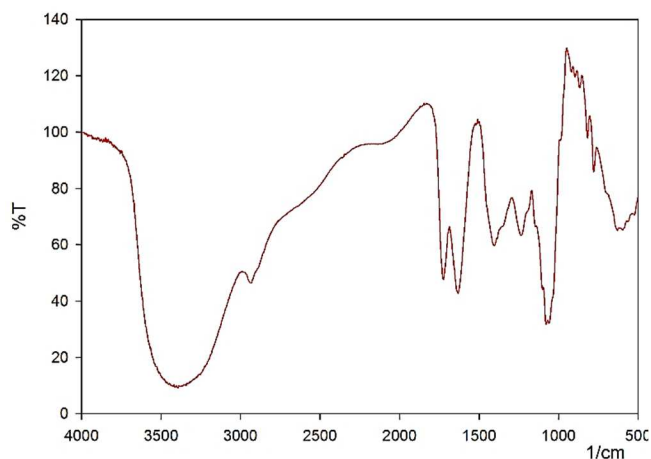


Fig. 7 FT-IR spectrum of strawberry extract

The particle size of TiO_2 powder was about 1000 nm as shown in Fig. 8. The size of these particles will affect the performance of the resulting solar cells. The presence of microscopic changes in the shape of the TiO_2 powder indicated that the TiO_2 paste had been successfully sintered. Based on Fig. 9, the TiO_2 paste particles formed pores. The pores were formed, which was caused by the addition of polyvinyl alcohol binder, which was then removed in the calcination so dye molecules could be adsorbed in the pores, which has implications for the performance of the resulting cells.

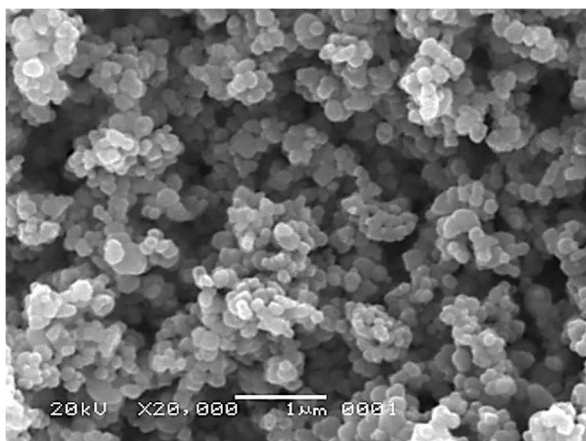


Fig. 8 SEM image of TiO_2 powder with 20,000 x magnification.

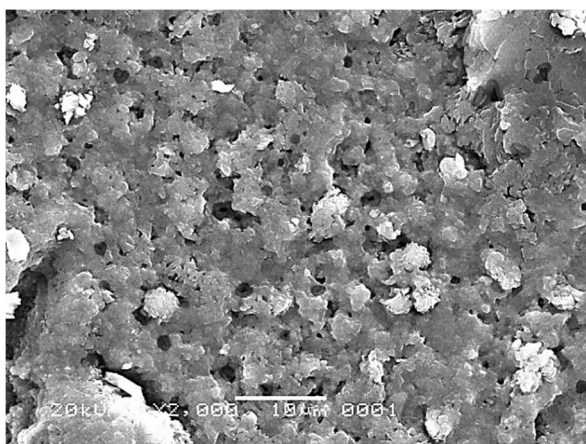


Fig. 9 SEM image of TiO_2 paste with 2,000 x magnification

Fig. 10 shows the comparison of the FTIR spectra of the TiO_2 semiconductor before and after immersion in dye. The emergence of new peaks indicated that the strawberry extract dye was successfully adsorbed on the TiO_2 semiconductor.

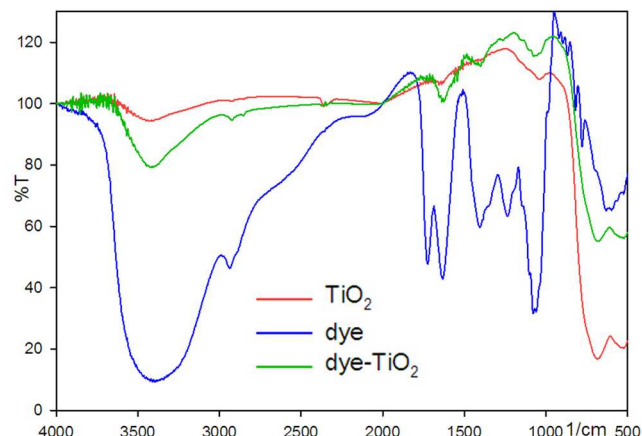


Fig. 10 Comparison of TiO_2 semiconductor FTIR spectra before and after soaking in strawberry extract dye

In Fig. 11, the current-voltage (I - V) characterization curve for Elt_1 was not yet ideal, where the curvature of the curve is still gentle. For Elt_2 and Elt_3 , the curve cannot be made because their currents and voltages were very small. Thus, they did not show maximum results when they connected to a potentiometer with varying resistance.

According to Table I, the V_{OC} that was produced by the prototype solar cell based on fatty imidazolium was quite significant at the laboratory scale so that fatty imidazolium can conduct ions [26]. Elt_1 has a better chance in voltage value than the comparison electrolyte due to the long alkyl chain [24] and the presence of double bonds [25] that allow electrostatic interactions. Therefore, the compound will form a liquid crystal phase (mesophases) [23] which can increase the I/I^{3-} transport rate by forming a self-assembly structure. It will prevent the charge recombination by the oxidized dye, so the efficiency was increased. The other two fatty imidazolium did not form mesophases; thus, the resulting cell voltage and ionic conductivity were also lower.

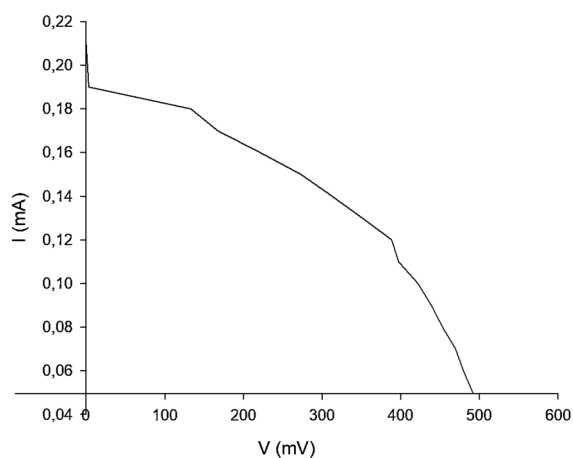


Fig. 11 Current vs. voltage of cis-oleyl-imidazolium iodide electrolyte

TABLE I
COMPARISON OF I_{sc} AND V_{oc} OF THE THREE FATTY IMIDAZOLIUM
ELECTROLYTES WITH COMPARISON ELECTROLYTE

Electrolyte Types	Composition	Ionic Liquid Addition	I_{sc} (mA)	V_{oc} (mV)
Comparison Electrolyte	I ₂ /KI in Acetonitrile	-	0.03	554
Elt ₁	I ₂ /KI in Acetonitrile	Cis-Oleyl Imidazolium Iodide	0.21	602
Elt ₂	I ₂ /KI in Acetonitrile	Palmityl-Imidazolium Iodide	0.004	427
Elt ₃	I ₂ /KI in Acetonitrile	Stearyl-Imidazolium Iodide	0.01	502

The particle size of the semiconductor used was still relatively large around 1000 nm (1 μ m) as shown in Fig. 12. It causes the surface area of the TiO₂ particles to be small, so the amount of dye adsorbed on the TiO₂ surface was relatively small. Therefore, the solar cell has low performance. TiO₂ paste that was deposited on the TCO glass was also very thick. The thickness of this paste affects the current generated by the solar cell, where the thicker the TiO₂ paste layer, the fewer electrons can flow into the TCO conductive glass layer because some of the electrons were recaptured by the oxidized dye. The electron injection in the conduction band of the TiO₂ semiconductor takes place on a femtosecond time scale, while dye regeneration takes place on a nanosecond time scale. These two processes compete with interfacial recombination of the semiconductor's conduction band that takes place on the nanoscale to milliseconds. So, the efficiency of DSSC solar cells depends on that competitive electron transfer kinetic and the DSSC prototype that was made (Fig. 13) also has a gap that allows the electrolyte to move when measured. This DSSC was characterized by a Solar Simulator of 100 mW/cm². The current-voltage characteristic of fatty imidazolium electrolytes was summarized in Table II.

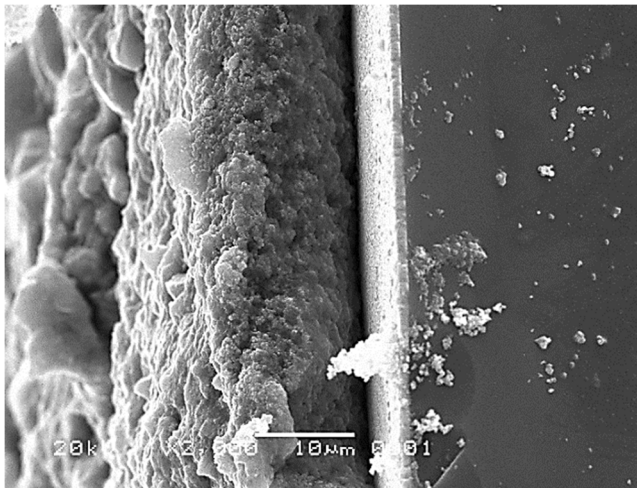


Fig. 12 Cross-section of TiO₂ paste deposited on TCO glass with 2,000 times magnification

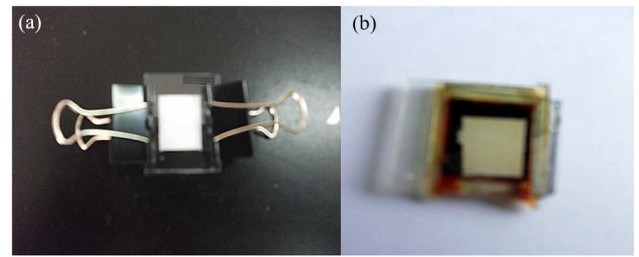


Fig. 13 (a) DSSC solar cell prototype device before electrolyte injection and (b) DSSC solar cell prototype device after electrolyte injection

TABLE II
CURRENT-VOLTAGE CHARACTERISTIC TEST RESULTS OF FATTY
IMIDAZOLIUM ELECTROLYTES

Parameters	Comparison Electrolyte	Elt ₁	Elt ₂	Elt ₃
V_{max} (mV)	-	388.5	-	-
P_{max} (mW)	-	46.62	-	-
P_{in} (mW/cm ²)	100	100	100	100
J_{sc} (mA/cm ²)	0.034	0.238	0.00455	0.011
V_{oc} (mV)	554	602	427	502
Fill Factor (%)	-	37	-	-
Efficiency (%)	0.07	0.53	0.00717	0.0203

B. Fabrication of DSSC Prototype Based on Graphite Waste Dispersed Composite Electrolytes

Because cis-oleyl-imidazolium iodide has the highest efficiency, therefore it was used for the composite redox electrolytes. These composite redox electrolytes did not add iodine from the outside, so this system was called an iodine-free system. The sonication was carried out to split the graphite into graphene sheets because ultrasonic energy can disrupt the electrostatic bond between layers. Graphite from a waste battery can be reused because this graphite was not different from synthetic graphite which has high purity.

Based on Table III, the conductivity of 0.05% addition of graphite was increased by more than 100% compared to the 0% graphite [34]. It seems that graphite was used as an electron transfer material. However, the addition of 0.1% graphite decreases the conductivity due to the added graphite already exceeds the solubility of graphite in ionic liquids. The presence of graphite that was not soluble may interfere with the ion conductivity of ionic liquids.

TABLE III
THE CONDUCTIVITY OF GRAPHITE DISPERSED 1,3-METHYL-OCTYL-1,2,3-
BENZOTRIAZOLIUM ACETATE

% Graphite	Voltage (Volt)	I (μ A)	Conductivity ($\times 10^{-6}$ S/cm)
0.00 %	5	30	1.35
0.01 %	5	121	3.85
0.05%	5	131	4.19
0.10 %	5	115	3.66

10% cis-oleyl imidazolium iodide could increase the conductivity by more than 100% compared to the conductivity of the 0% graphite which was shown in Table IV. The increased conductivity may cause by the cis-oleyl imidazolium iodide self-assembly structure that led to the regularity of the electron flow in electrical current delivery systems in this composite.

TABLE IV
THE CONDUCTIVITY OF 1,3-METHY-OCTYL- 1,2,3-BENZOTRIAZOLIUM
ACETATE WITH THE ADDING OF GRAPHITE AND 10% CIS-OLEYL
IMIDAZOLIUM IODIDE

% Graphite	Voltage (Volt)	I (μ A)	Conductivity ($\times 10^{-6}$ S/cm)
0.00 %	5	89	2.83
0.01 %	5	170	4.42
0.05 %	5	236	9.02
0.10 %	5	131	5.41

FTIR analysis on semiconductors aims to determine that the dye has been absorbed into the semiconductor by comparing the spectra of TiO_2 , Eosin Y, and the dye's immersed semiconductors. The combined spectra are shown in Fig. 14, indicating that Eosin Y has been successfully adsorbed into the TiO_2 semiconductor.

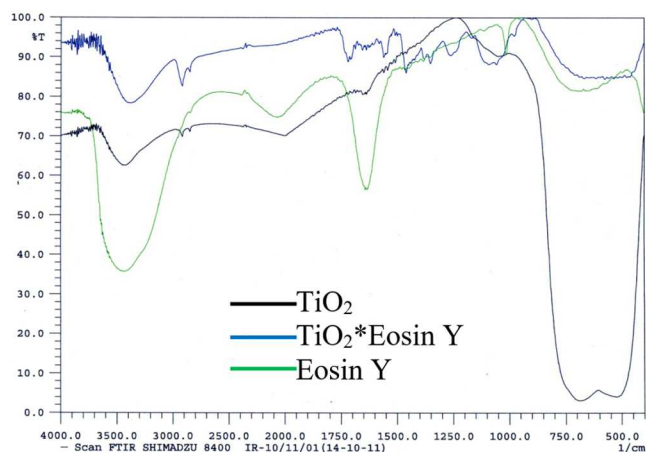


Fig. 14 Semiconductor spectra after immersion

The DSSCs of composite redox electrolytes were characterized by using Solar Simulator 16.6 mW/cm^2 . The current was so small that it cannot be measured on the measuring instrument, so a simulation was carried out to obtain the short circuit current using Microcal Origin 5 software by fitting current and voltage data. The graph of the current against voltage can be seen in Figs. 15-18.

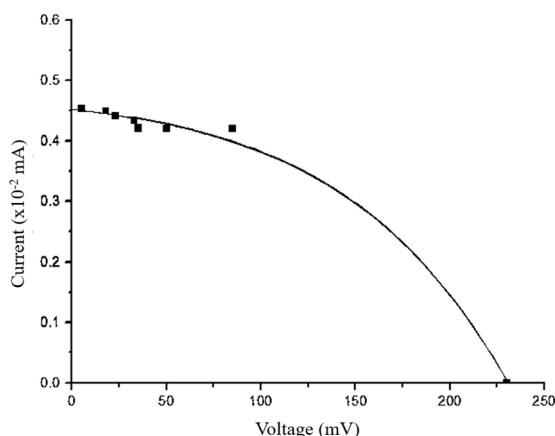


Fig. 15 DSSC with 0.00% graphite

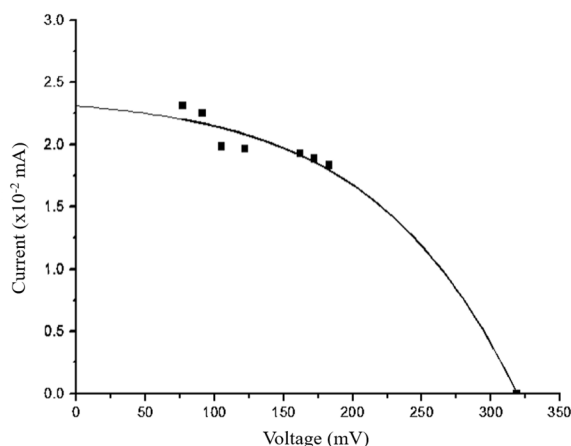


Fig. 16 Graph of DSSC with 0.01% graphite

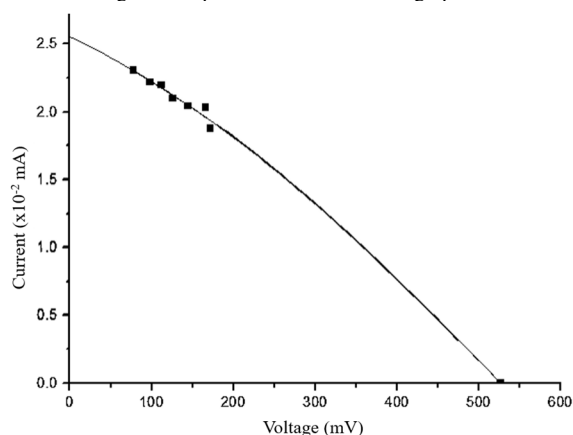


Fig. 17 Graph of DSSC with 0.05% graphite

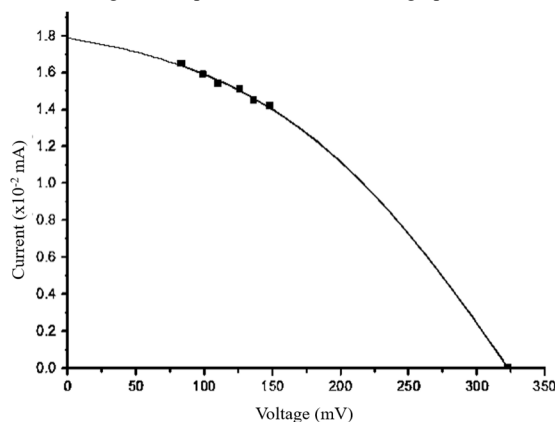


Fig. 18 Graph of DSSC with 0.10% graphite

Other parameters of DSSC were resulted by calculation from the graph and it was presented in Table V. The DSSC containing 0.05% of graphite exhibits a maximum short-circuit photocurrent density ($J_{SC} = 0.042 \text{ mA/cm}^2$), moderate open-circuit photovoltage ($V_{OC} = 527 \text{ mV}$) and an enhancement of the conversion efficiency ($\eta = 0.203\%$). Nevertheless, the greater fraction (0.10%) of graphite may interfere with the internal electron transportation routes or result in the electron back transportation from photoelectrode to counter electrode, which causes a poor performance (lower J_{SC} and η) of the DSSC. The availability of I^-/I_3^- redox coupling in the redox electrolyte was also another cause of the small current. The composite redox electrolytes relied solely on the supply of iodine from the added ionic liquid crystal,

and it affects the amount of current that was generated because when the dye gives electrons to the semiconductor, it must be immediately restabilized by the electrons from I/I^{3-} .

TABLE V
RESULT OF DSSC PARAMETER CALCULATION

Parameters	Elt ₄ 0% Graphite	Elt ₅ 0.01% Graphite	Elt ₆ 0.05% Graphite	Elt ₇ 0.10% Graphite
V_{max} (mV)	85	183	166	148
P_{max} ($\times 10^{-2}$ mW)	3.57	33	33.7	21
P_m (mW/cm ²)	16.6	16.6	16.6	16.6
J_{sc} (mA/cm ²)	0.0075	0.038	0.042	0.029
V_{oc} (mV)	230	319	527	323
I_{sc} ($\times 10^{-2}$ mA)	0.454	2.319	2.549	1.791
Fill Factor (%)	33	44	25	36
Efficiency (%)	0.02	0.198	0.203	0.126

So, Table V above shows the amount of iodine should be more than the amount of dye absorbed. The value of the fill factor (FF) of DSSCs that have been successfully fabricated was in the range of 25-44%, this corresponds to the shape of the current-voltage curve which was still sloping.

C. Exfoliation of Graphite into Graphene

Exfoliation of graphite into graphene was carried out to further analyze the potential of cis-oleyl-imidazolium acetate that enhanced DSSC efficiency. In graphite exfoliation by the dissolving method, ultrasonic energy was used to break the van der Waals interactions on carbon between graphite sheets to form graphene thin sheets. Before the ultrasonic energizing process, the graphite particles look larger and accumulate. But after the ultrasonic energizing process, the graphite particles look smaller and spread out between the solvents. This can be seen in Figs. 19 and 20. Meanwhile, the microwave was used to disrupt the electrostatic bond that occurs in the ionic liquid to maximize the dissolution of this exfoliation. The microwave energy in this exfoliation was very low to prevent damage to the mixture. After the microwave process, the graphite particles became smaller and dispersed between the cis-oleyl-imidazolium acetate compared to them before (see Fig. 21).

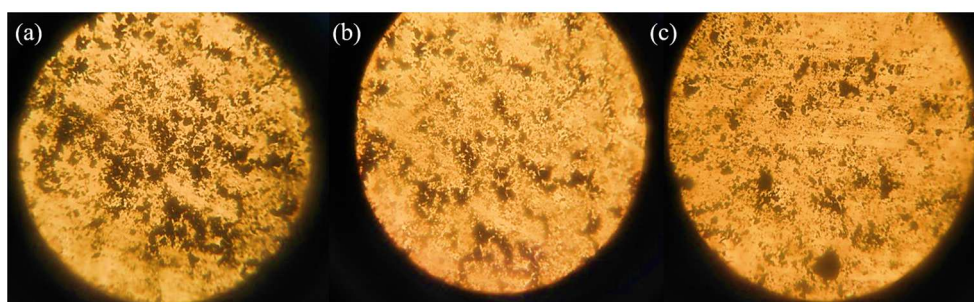


Fig. 19 (a) Synthetic graphite (b) waste battery graphite (c) new battery graphite viewed under a microscope with 400 times magnification before the sonication

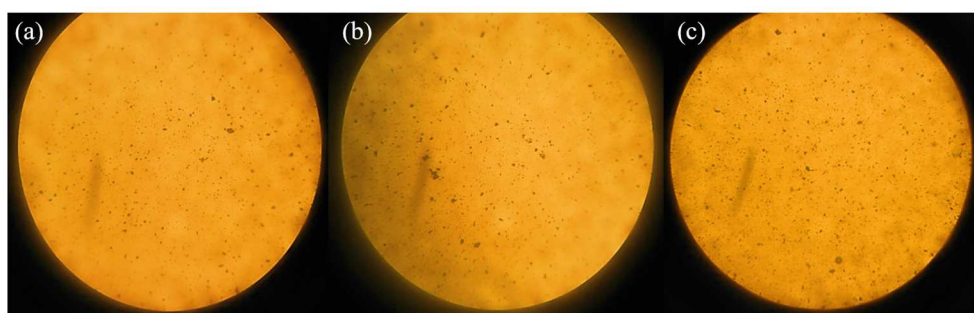


Fig. 20 (a) Synthetic graphite (b) waste battery graphite (c) new battery graphite viewed under a microscope with 400 times magnification after the sonication

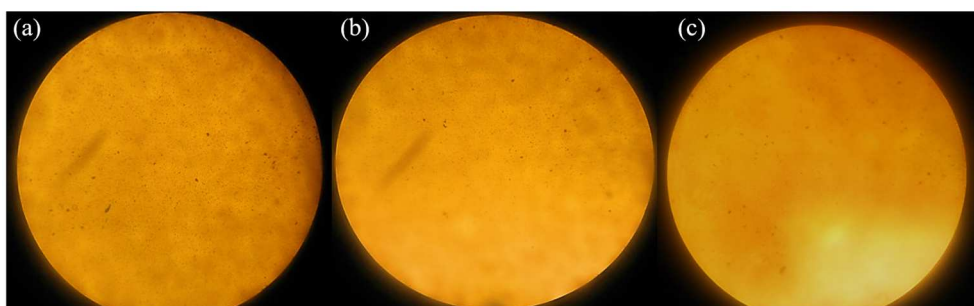


Fig. 21 (a) Synthetic graphite (b) waste battery graphite (c) new battery graphite viewed under a microscope with 400 times magnification after microwave

The sonication and microwave processes help penetration of cis-oleyl-imidazolium acetate into between the graphite sheets that accumulate, so the graphite sheets will be separated. In the electrochemical method, the greater applied stress allowed, the faster the graphite exfoliation. However, 15 V was the optimum voltage that could be applied for exfoliation by the electrochemical method. If it is more than 15 V, electrochemical instability will occur. Water in the fatty acid-based ionic liquid will affect the viscosity and conductivity of the ionic liquid because it will form new hydrogen bonds and reduce the cohesive energy, so the electrochemical window decreases. When an electric current was applied, the interaction of cations and anions caused a break in the van der Waals forces between the graphite planes, bubbles appeared in the cathode, then corrosion occurred in the anode, and a fine precipitate of exfoliated graphite was formed in the anode. The positive charge of the reduced fatty imidazolium cation in the cathode forms fatty imidazolium free radicals; thus, they can penetrate the bond in the graphite planes.

Fig. 22 shows a peak at 3411 cm^{-1} , which was the stretching vibration of the H-OH group originating from water molecules and it indicated that the graphite samples were not free from water molecules. Meanwhile, Fig. 23 shows the peak of C-H sp^2 stretching at 3003.9 cm^{-1} originating from stacking structures of exfoliated graphite. There was an absorption of 3317.3 cm^{-1} and a decrease in the intensity of C-H sp^3 stretching at 2900 and 2850 cm^{-1} because of the presence of exfoliated graphite in the ionic liquid. At 1647.5 cm^{-1} , there was a C=C stretching group which was a graphitic domain, and hydrophobic forces between ionic liquid and exfoliated graphite at $1400\text{-}800\text{ cm}^{-1}$ indicated a change in the graphite sample.

Figs. 24 and 25 show graphite diffractograms before and after exfoliation. In Fig. 24, there was a peak with the highest intensity, which is at $2\theta \pm 26.5$. Meanwhile, in Fig. 25, there was a change in the peak of the exfoliated graphite to $2\theta \pm 20$ which may be caused by the presence of ionic liquid that changes the structural composition of the graphite. This means that the ionic liquid was capable of penetrating the graphite structure, and multilayer graphene was formed.

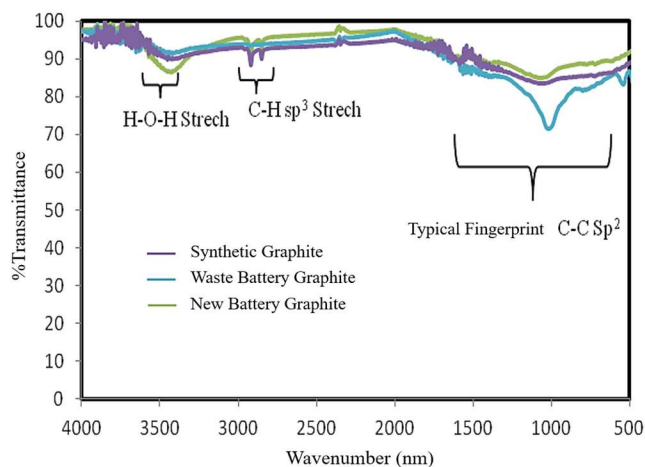


Fig. 22 Graphite FTIR spectrum before exfoliation

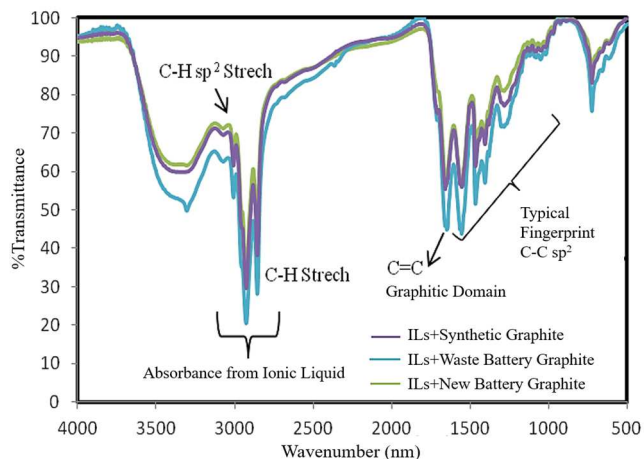


Fig. 23 Graphite FTIR spectrum after exfoliation

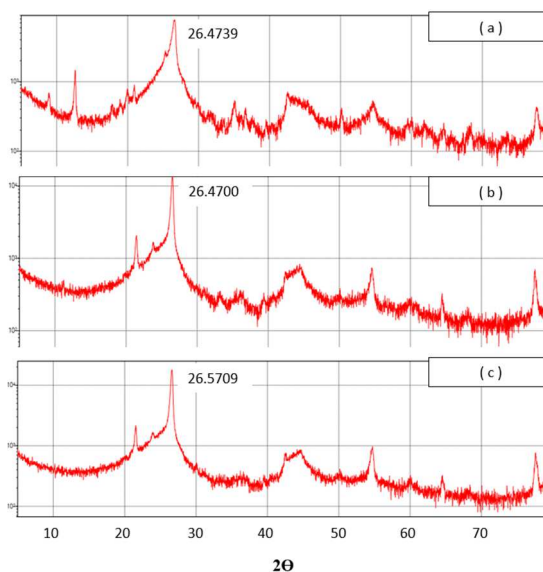


Fig. 24 Diffractogram of (a) waste battery graphite (b) synthetic graphite (c) new battery graphite before exfoliation

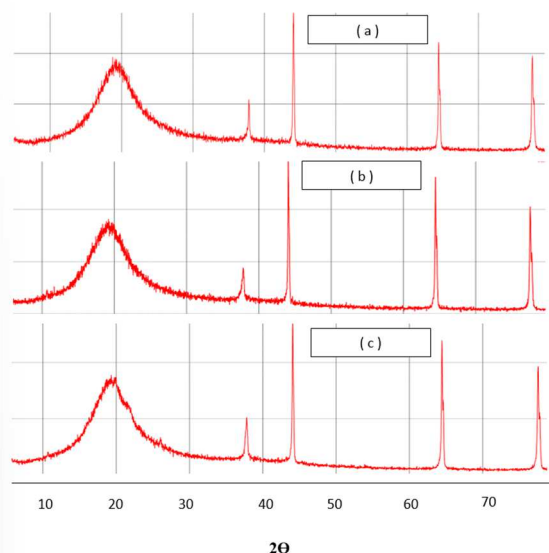


Fig. 25 Diffractogram (a) waste battery graphite (b) synthetic graphite (c) new battery graphite after exfoliation

Table VI shows that ionic liquids can decrease the crystallinity index of graphite. In Table VII, the graphite crystallite was decreased after the exfoliation. Based on Table VIII, the distance between layers of graphite becomes larger than before exfoliation. This means that the ionic liquid was able to penetrate the gaps between the graphite layers and stretch the distance between the layers.

Fig. 26 presents the surface morphology of the three graphite samples before and after the exfoliation. It can be concluded that there were structural and morphological changes on the surface of the three graphite samples. After exfoliation, the graphite was thinner and smoother than the graphite before the exfoliation, so the surface morphology of the graphite changed into a thinner flake, indicating the graphite exfoliation was successful. The thickness of multilayer graphene was produced from 300 to 3000 nm.

Before the exfoliation, the TG curve (Fig. 27) shows that the graphite begins to oxidize at 5000°C and then continues to decrease in mass by ~90% until 10000°C. This indicates that the graphite before exfoliation was stable above 5000°C. The graphite oxidation was accompanied by the release of energy as shown in the DTA curve (Fig. 28) where at 500-900°C, the curve increases, indicating an exothermic process. Meanwhile, on the TG (Fig. 29) and DTA (Fig. 30) curves, there were 3 stages of mass decomposition of the exfoliated graphite contained in the *cis*-oleyl-imidazolium acetate. In the first stage, there was a mass reduction of ~10% at 100-150°C due to the release of water molecules as impurities which was an endothermic process. In the second stage, there was a mass reduction of ~65% at 300-4000°C, indicating the decomposition of the *cis*-oleyl-imidazolium acetate. In the third stage, there was the oxidation of graphite which experienced a mass reduction of ~9.5 % starting at 5500°C and ending at 8000°C.

The Nyquist plot was made to explain the relationship between real impedance (Z_{real}) and imaginary impedance (Z_{im}) at a certain frequency where the greater resistance allowed the smaller conductivity. In Fig. 31, all graphite

components produce different resistance (R) at the same sample size.

TABLE VI
CRYSTALLINITY INDEX OF GRAPHITE

Sample	Condition	CI (%)
Waste Battery Graphite	Before	90.261438
Synthetic Graphite		94.298921
New Battery Graphite		94.991653
Waste Battery Graphite	After	73.255814
Synthetic Graphite		75.510204
New Battery Graphite		75.980392

TABLE VII
CRYSTALLITE SIZE OF GRAPHITE

Sample	Condition	Lc (Å)
Waste Battery Graphite	Before	1.2645685
Synthetic Graphite		1.224872
New Battery Graphite		1.3414189
Waste Battery Graphite	After	1.1955
Synthetic Graphite		1.2055
New Battery Graphite		1.3008

TABLE VIII
DISTANCE BETWEEN LAYERS OF GRAPHITE

Sample	Condition	$d_{(002)}$ (Å)	$d_{(002)}$ (nm)
Waste Battery Graphite	Before	3.365	0.3365
Synthetic Graphite		3.365	0.3365
New Battery Graphite		3.352	0.335
Waste Battery Graphite	After	4.450	0.445
Synthetic Graphite		4.468	0.446
New Battery Graphite		4.481	0.4481

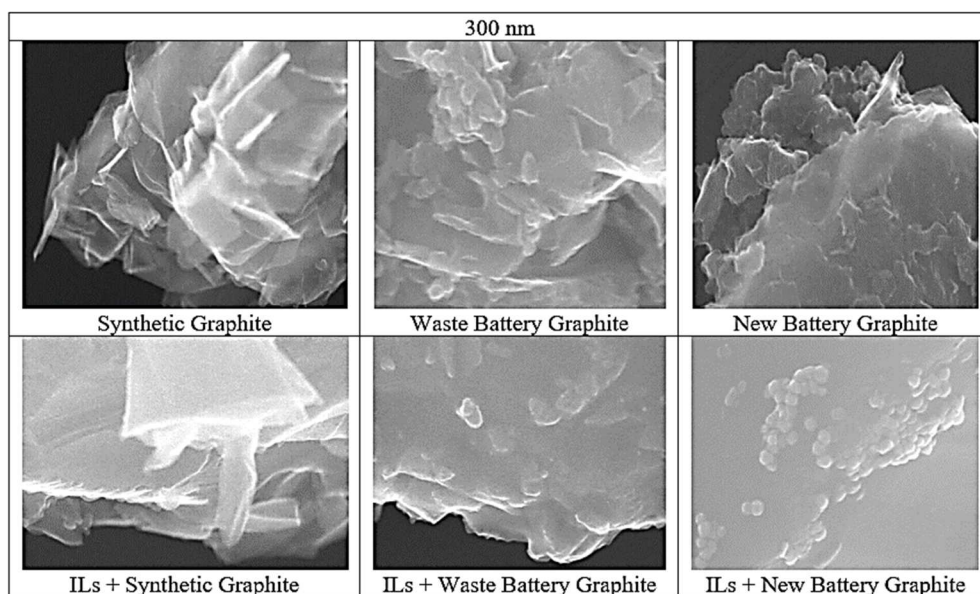


Fig. 26 The surface morphology of the three graphite samples before and after the exfoliation process using *cis*-oleyl-imidazolium ionic liquid

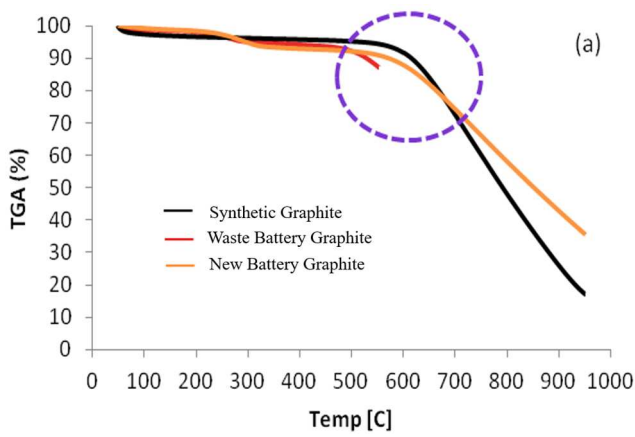


Fig. 27 Graphite TG curve before exfoliation

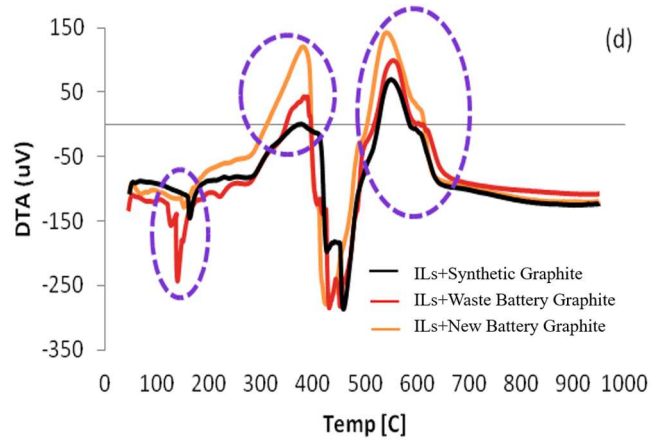


Fig. 30 Graphite DTA curve after exfoliation

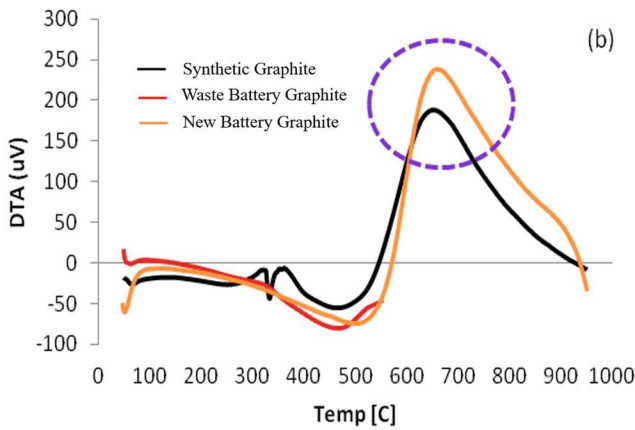


Fig. 28 Graphite DTA curve before exfoliation

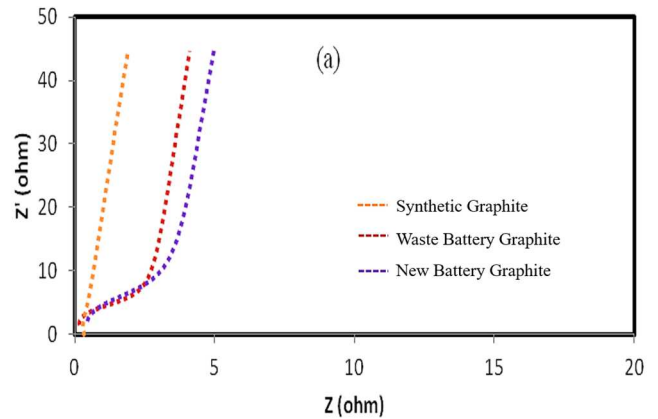


Fig. 31 Nyquist plot of graphite before exfoliation

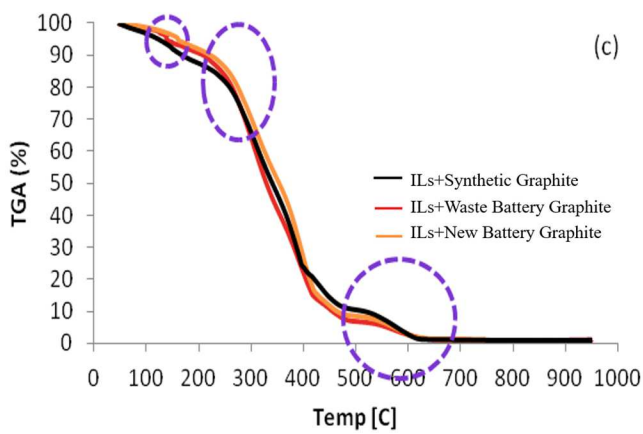


Fig. 29 Graphite TG curve after exfoliation

Waste battery graphite has a lower resistance than new battery graphite and synthetic graphite due to differences in the speed and amount of current flowing in the molecules that depend on the distance between the molecules. In solids, the smaller the distance between molecules, the easier electrons flow, and the resistance was getting smaller. The distance between the molecules in waste battery graphite was possibly getting smaller. Thus, the current flows faster with a large capacity. The vertical graph on the Nyquist plot shows the capacitive properties of the graphite sample. At low frequencies, graphite produces high resistance, but at high frequencies, graphite produces lower resistance. Thus, conductivity measurements were used at high frequencies.

Meanwhile, in Fig. 32, a typical semicircle curve was formed and also shows different resistances. The semicircle curve of exfoliated synthetic graphite has a narrower area than waste batteries and new batteries graphite. So, if the resistance was small, the faster the charge transfer will occur and the higher the conductivity.

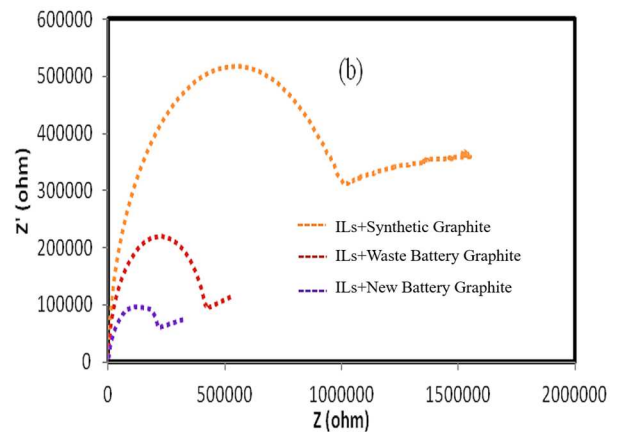


Fig. 32 Nyquist plot of graphite after exfoliation

Overall, graphite conductivity before and after exfoliation was presented in Table IX below. In synthetic graphite, the conductivity increased 10 times from 0.127 to 1.158 S/cm, and the waste battery graphite increased twice from 0.364 to 0.796 S/cm, while the graphite of the new battery increased 4 times from 0.205 to 0.932 S/cm. Compared to the ionic liquid's conductivity, the exfoliated graphite increases

drastically. This means that the exfoliation can increase the conductivity of graphite and indicates that the exfoliation of graphite into graphene was successful.

TABLE IX
GRAPHITE CONDUCTIVITY BEFORE AND AFTER EXFOLIATION

Sample	R ₁ (ohm)	Conductivity (S/cm)
Synthetic Graphite	0.445	1.27 x 10 ⁻¹
New Battery Graphite	0.31	2.05 x 10 ⁻¹
Waste Battery Graphite	0.155	3.64 x 10 ⁻¹
ILs + Synthetic Graphite	33	11.58 x 10 ⁻¹
ILs + New Battery Graphite	41	9.32 x 10 ⁻¹
ILs + Waste Battery Graphite	48	7.96 x 10 ⁻¹
ILs	1375	9.26 x 10 ⁻⁵

Note: ILs = Cis-oleyil-imidazolium acetate ionic liquid

IV. CONCLUSION

This research successfully investigated ionic liquids as a composite redox electrolyte for DSSC. Cis-oleyil-imidazolium iodide has the highest efficiency (0.053%) among stearyl or palmityl-imidazolium iodide due to its longest alkyl chains and a double bond. So, cis-oleyil-imidazolium was used along with 1,3-methyloctyl-1,2,3-benzotriazolium acetate and graphite as composite redox electrolytes like cocktails. Dispersion of 0.05% of the graphite result in an efficiency enhancement (about 100%), but the greater fraction (0.1%) of the graphite causes a poor performance possibly due to interference of the internal electron transportation routes by insoluble graphite. Then, graphite exfoliation into graphene using cis-oleyil-imidazolium acetate has been studied for better enhancement. It was known that cis-oleyil-imidazolium acetate could enhance the conductivity of synthetic graphite, new battery graphite, and waste battery graphite up to 10, 4, and 2 times respectively. Thus, cis-oleyil-imidazolium acetate as a composite redox electrolyte for DSSC needs to be evaluated further.

ACKNOWLEDGMENT

The financial support from Indonesian Governments (RISTEK BRIN) is gratefully acknowledged.

REFERENCES

- [1] N. Mariotti, M. Bonomo, L. Fagiolari, N. Barbero, C. Gerbaldi, F. Bella, and C. Barolo, "Recent advances in eco-friendly and cost-effective materials towards sustainable dye-sensitized solar cells," *Green Chemistry*, vol. 22, no. 21, pp. 7168-7218, July, 2020.
- [2] F. Ahmad, N. Qurban, Z. Fatima, T. Ahmad, I. Zahid, A. Ali, S. R. Rajpoot, M. W. Tasleem, and E. Maqbool, "Electrical characterization of II-VI thin films for solar cells application," *ASEAN Journal of Science and Engineering Education*, vol. 2, no. 2, pp. 199-208, Oct. 2022.
- [3] A. K. Irawan, D. Rusdiana, W. Setiawan, W. Purnama, R. M. Fauzi, S. A. Fauzi, A. H. F. Alfani, and M. R. Arfiyogo, "Design-construction of a solar cell energy water pump as a clean water source for people in sirnajaya village, gununghalu district," *ASEAN Journal of Science and Engineering Education*, vol. 1, no. 1, pp. 15-20, Feb. 2021.
- [4] J. M. Cole, G. Pepe, O. K. Al Bahri, and C. B. Cooper, "Cosensitization in Dye-Sensitized Solar Cells," *Chem. Rev.*, vol. 119, no. 12, pp. 7279-7327, 2019.
- [5] C. Banne, "Modern third generation solar photovoltaic technology: Dye sensitized solar cell," *J. Mech. Energy Eng.*, vol. 4, no. 2, pp. 173-178, Nov. 2020.

- [6] M. Z. Toe, S. Y. Pung, K. A. Yaacob, A. Matsuda, W. K. Tan, and S. S. Han, "Effect of TiO₂ sol on the conversion efficiency of TiO₂ based dye-sensitized solar cell," *J. Sol-Gel Sci. Technol.*, vol. 95, no. 2, pp. 439-446, Aug. 2020.
- [7] A. Khalifa *et al.*, "Comprehensive performance analysis of dye-sensitized solar cells using single layer TiO₂ photoanode deposited using screen printing technique," *Optik (Stuttg.)*, vol. 223, p. 165595, Dec. 2020.
- [8] S. N. Karthick, K. V. Hemalatha, Suresh Kannan Balasingam, F. Manik Clinton, S. Akshaya, and H. Kim, "Dye-Sensitized Solar Cells: History, Components, Configuration, and Working Principle," in *Interfacial Engineering in Functional Materials for Dye-Sensitized Solar Cells*, Wiley, pp. 1-16, 2019.
- [9] M. M. Abdel-Galeil, R. Kumar, A. Matsuda, and R. E. El-Shater, "Investigation on influence of thickness variation effect of TiO₂ film, spacer and counter electrode for improved dye-sensitized solar cells performance," *Optik (Stuttg.)*, vol. 227, p. 166108, Feb. 2021.
- [10] F. I. Chowdhury, M. H. Buraidah, A. K. Arof, B.-E. Mellander, and I. M. Noor, "Impact of tetrabutylammonium, iodide and triiodide ions conductivity in polyacrylonitrile based electrolyte on DSSC performance," *Sol. Energy*, vol. 196, pp. 379-388, 2020.
- [11] A. M. Zulkifli *et al.*, "Characteristics of Dye-Sensitized Solar Cell Assembled from Modified Chitosan-Based Gel Polymer Electrolytes Incorporated with Potassium Iodide," *Molecules*, vol. 25, no. 18, 2020.
- [12] C. Xu, X. Zhao, M. Sun, J. Ma, and M. Wu, "Highly effective 2D layered carbides counter electrode for iodide redox couple regeneration in dye-sensitized solar cells," *Electrochim. Acta*, vol. 392, p. 138983, Oct. 2021.
- [13] S. Venkatesan, I.-P. Liu, C.-M. Tseng Shan, H. Teng, and Y.-L. Lee, "Highly efficient indoor light quasi-solid-state dye sensitized solar cells using cobalt polyethylene oxide-based printable electrolytes," *Chem. Eng. J.*, vol. 394, p. 124954, 2020.
- [14] S. Balamurugan and S. Ganesan, "Novel cobalt redox materials admitted in natrosol polymer with a thiophene based additive as a gel polymer electrolyte to tune up the efficiency of dye sensitized solar cells," *Electrochim. Acta*, vol. 329, p. 135169, Jan. 2020.
- [15] J.-D. Peng, Y.-T. Wu, M.-H. Yeh, F.-Y. Kuo, R. Vittal, and K.-C. Ho, "Transparent Cobalt Selenide/Graphene Counter Electrode for Efficient Dye-Sensitized Solar Cells with Co 2+ / 3+ -Based Redox Couple," *ACS Appl. Mater. Interfaces*, vol. 12, no. 40, pp. 44597-44607, Oct. 2020.
- [16] K. Yang, X. Yang, L. Zhang, J. An, H. Wang, and Z. Deng, "Copper redox mediators with alkoxy groups suppressing recombination for dye-sensitized solar cells," *Electrochim. Acta*, vol. 368, p. 137564, 2021.
- [17] A. Colombo, C. Dragonetti, D. Roberto, and F. Fagnani, "Copper complexes as alternative redox mediators in dye-sensitized solar cells," *Molecules*, vol. 26, no. 1, 2021.
- [18] T. Higashino, H. Iiyama, S. Nimura, Y. Kurumisawa, and H. Imahori, "Effect of Ligand Structures of Copper Redox Shuttles on Photovoltaic Performance of Dye-Sensitized Solar Cells," *Inorg. Chem.*, vol. 59, no. 1, pp. 452-459, Jan. 2020.
- [19] R. A. A. Talip, W. Z. N. Yahya, and M. A. Bustam, "Ionic liquids roles and perspectives in electrolyte for dye-sensitized solar cells," *Sustainability (Switzerland)*, vol. 12, no. 18, Sep. 2020.
- [20] J. E. Sitanggang, N. Z. Latifah, O. Sopian, Z. Saputra, A. B. D. Nandiyanto, S. Anggraeni, and A. Rahmat, "Analysis of cassava peel and pineapple peel as electrolytes in bio battery," *Indonesian Journal of Multidisciplinary Research*, vol. 1, no. 1, pp. 59-62, 2021.
- [21] A. M. Nurjamil, N. A. Wolio, R. N. Laila, S. A. Rohmah, S. Anggraeni, and A. B. D. Nandiyanto, "Effect of rice husks and wood grain as electrolyte adsorbers on battery," *Indonesian Journal of Multidisciplinary Research*, vol. 1, no. 1, pp. 69-72, 2021.
- [22] H. Syawal, N. K. Farhana, Z. L. Goh, S. Bashir, N. M. Saidi, E. Rachagan, S. Ramesh, and R. Kasi, "Highly efficient dye-sensitized solar cells: A comparative study with two different system of solvent-free binary room-temperature ionic liquid-based electrolytes," *J. Appl. Polym. Sci.*, vol. 138, no. 44, p. 51312, Nov. 2021.
- [23] G. Bousrez, O. Renier, B. Adranno, V. Smetana, and A. V. Mudring, "Ionic Liquid-Based Dye-Sensitized Solar Cells - Insights into Electrolyte and Redox Mediator Design," *ACS Sustain. Chem. Eng.*, vol. 9, no. 24, pp. 8107-8114, Jun. 2021.
- [24] D. Song, Y. S. Choi, B. S. Kim, H. S. Kim, and Y. S. Kang, "Size effects of imidazolium cations bearing cyanoethyl group on performance of dye-sensitized solar cells," *Mater. Lett.*, vol. 246, pp. 137-140, 2019.

- [25] Y. Fang *et al.*, "Synthesis of low-viscosity ionic liquids for application in dye-sensitized solar cells," *Chem. - An Asian J.*, vol. 14, no. 23, pp. 4201–4206, Dec. 2019.
- [26] A. Syairah, M. H. Khanmirzaei, N. M. Saidi, N. K. Farhana, S. Ramesh, and K. Ramesh, "Effect of different imidazolium-based ionic liquids on gel polymer electrolytes for dye-sensitized solar cells," *Ionics (Kiel)*, vol. 25, no. 5, pp. 2427–2435, May 2019.
- [27] L. A. Santa-Cruz *et al.*, "Effect of heterocyclic nitrogen ionic liquid additives on the rate of backreaction in DSSCs: An electrochemical characterization," *J. Sci. Adv. Mater. Devices*, vol. 6, no. 3, pp. 483–487, Sep. 2021.
- [28] J. Y. Kim, K. H. Kim, D.-H. Kim, and Y. S. Han, "Effects of a dianion compound as a surface modifier on the back reaction of photogenerated electrons in TiO₂-based solar cells," *Arab. J. Chem.*, vol. 13, no. 1, pp. 2340–2348, Jan. 2020.
- [29] D. A. Chalkias, D. D. Loizos, and G. C. Papanicolaou, "Evaluation and prediction of dye-sensitized solar cells stability under different accelerated ageing conditions," *Sol. Energy*, vol. 207, pp. 841–850, Sep. 2020.
- [30] N. Narudin, P. Ekanayake, Y. W. Soon, H. Nakajima, and C. M. Lim, "Enhanced properties of low-cost carbon black-graphite counter electrode in DSSC by incorporating binders," *Sol. Energy*, vol. 225, pp. 237–244, Sep. 2021.
- [31] R. R. Sunarya, R. Hidayat, C. L. Radiman, and V. Suendo, "Electrocatalytic activation of a DSSC graphite composite counter electrode using in situ polymerization of aniline in a water/ethanol dispersion of reduced graphene oxide," *J. Electron. Mater.*, vol. 49, no. 5, pp. 3182–3190, May 2020.
- [32] M. F. Don, P. Ekanayake, H. Nakajima, A. H. Mahadi, C. M. Lim, and A. Atod, "Acetylene carbon black-graphite composite as low-cost and efficient counter electrode for dye-sensitized solar cells (DSSCs)," *Ionics (Kiel)*, vol. 25, no. 11, pp. 5585–5593, Nov. 2019.
- [33] Ristiana, Q.A, "Electrical textile: graphite paste on gloves for touching screen of smartphones and tablets," *ASEAN Journal for Science and Engineering in Materials*, vol. 1, no. 1, pp. 13-20, 2022.
- [34] D. Krishnan, N. S. Powar, A. Vasanth, K. V. Ramanathan, S. V. Nair, and M. Shanmugam, "Graphene oxide enabled hole transport characteristics in iodide/tri-iodide for improved dye sensitized solar cell performance," *Mater. Lett.*, vol. 285, Feb. 2021.
- [35] S. Mahalingam *et al.*, "Functionalized graphene quantum dots for dye-sensitized solar cell: Key challenges, recent developments and future prospects," *Renew. Sustain. Energy Rev.*, vol. 144, p. 110999, Jul. 2021.
- [36] E. Muchuweni, B. S. Martincigh, and V. O. Nyamori, "Recent advances in graphene-based materials for dye-sensitized solar cell fabrication," *RSC Adv.*, vol. 10, no. 72, pp. 44453–44469, 2020.
- [37] D. Bajpai and V. K. Tyagi, "Microwave synthesis of cationic fatty imidazolines and their characterization," *J. Surfactants Deterg.*, vol. 11, no. 1, pp. 79–87, Mar. 2008.
- [38] S. A. Forsyth and D. R. MacFarlane, "1-alkyl-3-methylbenzotriazolium salts: ionic solvents and electrolytes," *J. Mater. Chem.*, vol. 13, no. 10, pp. 2451–2456, 2003.
- [39] R.A. Pratiwi; and A.B.D. Nandiyanto, "How to read and interpret UV-VIS spectrophotometric results in determining the structure of chemical compounds", *Indonesian Journal of Educational Research and Technology*, vol. 2, no. 1, pp. 1-20, 2022.
- [40] A.B.D. Nandiyanto; R. Oktiani; and R. Ragadhita, "How to read and interpret FTIR spectroscopy of organic material", *Indonesian Journal of Science and Technology*, vol. 4, no. 1, pp. 97-118, 2019.
- [41] S. Fatimah; R. Ragadhita; D.F. Al Husaeni; and A.B.D. Nandiyanto, "How to calculate crystallite size from x-ray diffraction (XRD) using Scherrer method", *ASEAN Journal of Science and Engineering*, vol. 2, no. 1, pp. 65-76, 2022.
- [42] Y.D. Yolanda; and A.B.D. Nandiyanto, "How to read and calculate diameter size from electron microscopy images", *ASEAN Journal of Science and Engineering Education*, vol. 2, no. 1, pp. 11-36, 2022.
- [43] R. Ragadhita; and A.B.D. Nandiyanto, "Why 200°C is effective for creating carbon from organic waste (from thermal gravity (TG-DTA) perspective)?" , vol. 2, no. 2, pp. 75-80, 2023.
- [44] N. K. Farhana, N. M. Saidi, S. Bashir, S. Ramesh, and K. Ramesh, "Review on the Revolution of Polymer Electrolytes for Dye-Sensitized Solar Cells," *Energy and Fuels*, vol. 35, no. 23, pp. 19320–19350, Dec. 2021.
- [45] K. F. Chan, H. N. Lim, H. Ahmad, and N. S. K. Gowthaman, "Photovoltaic performance of bipyridine and dipyrrophenazine ligands anchored ruthenium complex sensitizers for efficient dye-sensitized solar cells," *Solid State Sci.*, vol. 107, p. 106368, 2020.